

Guaranteed Velocity Error Control for the Pseudostress Approximation of the Stokes Equations

P. Bringmann,¹ C. Carstensen,¹ C. Merdon²

¹Department of Mathematics, Humboldt-Universität zu Berlin, Unter den Linden 6, 10099 Berlin, Germany

²Weierstrass Institute for Applied Analysis and Stochastics, Mohrenstrasse 39, 10117 Berlin, Germany

Received 11 March 2015; accepted 4 February 2016

Published online 4 May 2016 in Wiley Online Library (wileyonlinelibrary.com).

DOI 10.1002/num.22056

The pseudostress approximation of the Stokes equations rewrites the stationary Stokes equations with pure (but possibly inhomogeneous) Dirichlet boundary conditions as another (equivalent) mixed scheme based on a stress in $H(\text{div})$ and the velocity in L^2 . Any standard mixed finite element function space can be utilized for this mixed formulation, e.g., the Raviart-Thomas discretization which is related to the Crouzeix-Raviart nonconforming finite element scheme in the lowest-order case. The effective and guaranteed a posteriori error control for this nonconforming velocity-oriented discretization can be generalized to the error control of some piecewise quadratic velocity approximation that is related to the discrete pseudostress. The analysis allows for local inf-sup constants which can be chosen in a global partition to improve the estimation. Numerical examples provide strong evidence for an effective and guaranteed error control with very small overestimation factors even for domains with large anisotropy. © 2016 Wiley Periodicals, Inc. Numer Methods Partial Differential Eq 32: 1411–1432, 2016

Keywords: a posteriori error estimation; adaptive finite element method; Crouzeix-Raviart element; nonconforming finite element method; pseudostress finite element method; Stokes equations

I. INTRODUCTION

The pseudostress finite element method (PS-FEM) has recently been established in the context of a least-squares finite element method for the Stokes equations [1–3]. The adaptive mesh-refinement leads to optimal convergence rates [4] for the lowest-order case. This and the principle availability for higher polynomial degrees makes this mixed finite element method highly attractive over the nonconforming P_1 finite element method usually attributed to Crouzeix and Raviart.

The error control for finite element methods in the energy norm with residual-based explicit error estimators typically leads to unknown or large multiplicative reliability constants and is

Correspondence to: C. Carstensen, Humboldt-Universität zu Berlin, Berlin, Germany (e-mail: cc@math.hu-berlin.de)

Contract grant sponsor: Deutsche Forschungsgemeinschaft (DFG) Research Center MATHEON

Contract grant sponsor: Berlin Mathematical School (BMS)

© 2016 Wiley Periodicals, Inc.

usually uncompetitive over refined methodologies like equilibration error estimators that lead to guaranteed upper bounds, see [5–7] for recent error estimator competitions. The error analysis of nonconforming finite element schemes concerns the geometric condition that one variable is a distributional gradient of an H^1 -function. It thereby involves the design of a particular test function v near to the discrete solution u_h . For the Stokes problem, the side conditions on this Sobolev function require the match of the true Dirichlet boundary conditions as well as the incompressibility condition $\operatorname{div} v = 0$ a.e. in the domain Ω . The relaxation of this later condition has been suggested in [8] based on some regular split of a gradient into a gradient of a divergence-free H^1 function and an L^2 -orthogonal remainder. If a lower bound of the inf-sup constant c_0 from Subsection II.A is known, this regular split leads to the guaranteed upper bound of the energy error

$$\| \|u - u_h\|_{\text{NC}}^2 \leq \eta^2 + (\| \|v - u_h\|_{\text{NC}} + \|\operatorname{div} v\|_{L^2(\Omega)}/c_0)^2.$$

The first quantity η depends only on the right-hand side f , while the second term on the right-hand side depends on v . Another advantage of the PS-FEM is the appearance of the oscillation of the right-hand side f in η compared to the L^2 -norm of the mesh-size times f in the nonconforming case [9]. The stability constant c_0 is an inf-sup constant and difficult to compute, see [10] and [11] for the corrected results. Moreover, c_0 deteriorates for stretched domains with large aspect ratios [12] and so may crucially worsen the efficiency indices of all error estimators based on designs of non divergence-free test functions. Several such designs were proposed and compared in [8, 13, 14] and mainly stem from popular conforming postprocessings of nonconforming finite element solutions for the Poisson problem [15–17, 7].

The localization technique [9] allows a partition $\Omega_1, \dots, \Omega_J$ of Ω with (practical) inf-sup constants c_j of Ω_j and leads to guaranteed upper bounds that only include the local inf-sup constants, i.e.,

$$\| \|u - u_h\|_{\text{NC}}^2 \leq \eta^2 + \sum_{j=1}^J (\| \mathbb{D}_{\text{NC}}(v - u_h) \|_{L^2(\Omega_j)} + \|\operatorname{div} v\|_{L^2(\Omega_j)}/c_j)^2.$$

However, this is only valid if the designed test function v satisfies the additional condition

$$\int_{\partial\Omega_j} v \cdot \nu_{\Omega_j} \, ds = 0 \quad \text{for } j = 1, \dots, J.$$

To mention just two prominent situations, one may think of a decomposition of an L-shaped domain or a long thin channel into squares. Moreover, the localization technique can produce guaranteed error bounds even when (lower bounds of) the global inf-sup constants are unknown, e.g. for the backward facing step example.

Section IV presents several strategies of how to satisfy the additional constraint within the test function designs from [13] in more detail than in [9]. Section IV.E suggests a universal projection that works for any test function designs, in particular for combination with solutions from (truncated) global minimization problems. An additional lumping in the projection matrix renders this technique very inexpensive.

The resulting error estimators are studied for the lowest-order PS-FEM, where $u_h := u_2$ is some piecewise quadratic function whose piecewise gradient equals (up to some pressure contribution) the approximation σ_{PS} of the exact pseudostress σ in the pseudostress finite element space $\text{PS}(\mathcal{T})$ of Section III. The L^2 -error $\sigma - \sigma_{\text{PS}}$ is quasi-optimal [4, 18] in the sense that

$$\| \sigma - \sigma_{\text{PS}} \|_{L^2(\Omega)} \lesssim \inf_{\tau_{\text{PS}} \in \text{PS}(\mathcal{T})} \| \sigma - \tau_{\text{PS}} \|_{L^2(\Omega)} + \operatorname{osc}(f, \mathcal{T}).$$

The proposed error estimator designs of the present article lead to the sharpest guaranteed upper error bounds known for this scheme, even in the case of challenging domains with very small inf-sup constants.

The remaining parts of this article are organized as follows. Section II recalls the Stokes equations and describes the nonconforming finite element discretization. Section III presents the pseudostress approximation and states the main result for the guaranteed upper error bound in Theorem 3.1 on page 6. Section IV designs different interpolations of the discrete velocity which lead to guaranteed upper error bounds. It includes the treatment of inhomogeneous Dirichlet boundary conditions. Finally, Section V presents numerical experiments on some benchmark problems.

The article is written in the 2D case although the arguments for the main result in Theorem 3.1 carry over to the 3D case as well. However, the designs of appropriate test functions are more involved.

Standard notation on Lebesgue and Sobolev spaces applies throughout this article such as $H^k(\Omega)$, $H(\text{div}, \Omega)$, and $L^2(\Omega)$ and the associated spaces for vector- or matrix-valued functions $H^k(\Omega; \mathbb{R}^2)$, $L^2(\Omega; \mathbb{R}^2)$, $H^k(\Omega; \mathbb{R}^{2 \times 2})$, $H(\text{div}, \Omega; \mathbb{R}^{2 \times 2})$, and $L^2(\Omega; \mathbb{R}^{2 \times 2})$. Let $H_0^1(\Omega) := \{v \in H^1(\Omega) : v \equiv 0 \text{ on } \partial\Omega \text{ in the sense of traces}\}$ be equipped with the energy norm

$$\| \cdot \| := | \cdot |_{H^1(\Omega)} = \| \mathbf{D} \cdot \|_{L^2(\Omega)} .$$

The 2D rotation operators read, for $v \in H^1(\Omega; \mathbb{R}^2)$,

$$\text{Curl } v := \begin{pmatrix} -\partial v_1 / \partial x_2 & \partial v_1 / \partial x_1 \\ -\partial v_2 / \partial x_2 & \partial v_2 / \partial x_1 \end{pmatrix} \quad \text{and} \quad \text{curl } v := \text{tr Curl } v .$$

The expression $A \lesssim B$ abbreviates the relation $A \leq CB$ with a generic constant $0 < C$ which solely depends on the interior angles $\angle \mathcal{T}$ of the underlying triangulation; $A \approx B$ abbreviates $A \lesssim B \lesssim A$.

II. NOTATION AND PRELIMINARIES

A. Stokes Equations

This article concerns the 2D Stokes equations: Given a right-hand side $f \in L^2(\Omega; \mathbb{R}^2)$ and Dirichlet boundary data $u_D \in H^1(\Omega; \mathbb{R}^2)$ with $\int_{\partial\Omega} u_D \cdot \nu \, ds = 0$, seek a pressure $p \in L_0^2(\Omega; \mathbb{R}^2) := \{q \in L^2(\Omega; \mathbb{R}^2) : \int_{\Omega} q \, dx = 0\}$ and a velocity field $u \in H^1(\Omega; \mathbb{R}^2)$ with

$$-\Delta u + \nabla p = f \quad \text{and} \quad \text{div } u = 0 \text{ in } \Omega \quad \text{while} \quad u = u_D \text{ on } \partial\Omega .$$

The error analysis involves (lower bounds of) the inf-sup constant

$$0 < c_0 := \inf_{q \in L_0^2(\Omega) \setminus \{0\}} \sup_{v \in H_0^1(\Omega; \mathbb{R}^2) \setminus \{0\}} \int_{\Omega} q \, \text{div } v \, dx / (\| \mathbf{D} v \|_{L^2(\Omega)} \| q \|_{L^2(\Omega)})$$

of the Ladyzhenskaya lemma [19, §6. Theorem 6.3] and depends on Ω . Lower bounds for this constant are in general difficult to compute; see [10] and for corrected results [11]. Recall from [12], that c_0 deteriorates for stretched domains with large anisotropy. Section III explains remedies for these problems based on [9].

B. Nonconforming Finite Element Spaces

Given a regular triangulation \mathcal{T} of the bounded Lipschitz domain $\Omega \subseteq \mathbb{R}^2$ into closed triangles in the sense of Ciarlet with the set of edges \mathcal{E} and the set of nodes \mathcal{N} . Let $\mathcal{E}(\Omega)$ resp. $\mathcal{N}(\Omega)$ denote the set of interior edges resp. the set of interior nodes. The set of edges along the boundary $\partial\Omega$ reads $\mathcal{E}(\partial\Omega)$ and the set of boundary nodes $\mathcal{N}(\partial\Omega)$. Define the set $\text{mid}(\mathcal{E}) := \{\text{mid}(E) : E \in \mathcal{E}\}$ of midpoints of all edges and let $\mathcal{E}(T)$ be the set of the three edges and $\mathcal{N}(T)$ the set of the three vertices of a triangle $T \in \mathcal{T}$. Let the set $\mathcal{T}(z)$ contain all triangles $T \in \mathcal{T}$ with vertex $z \in \mathcal{N}(T)$ for a node $z \in \mathcal{N}$ and denote its cardinality with $|\mathcal{T}(z)|$. The diameter $\text{diam}(T)$ of $T \in \mathcal{T}$ is denoted by h_T and $h_{\mathcal{T}}$ denotes their piecewise constant values with $h_{\mathcal{T}|_T} := h_T := \text{diam}(T)$ for all $T \in \mathcal{T}$. With the elementwise polynomials $P_k(\mathcal{T}; \mathbb{R}^2)$ of degree at most k , the nonconforming Crouzeix-Raviart finite element spaces read

$$\begin{aligned} \text{CR}^1(\mathcal{T}; \mathbb{R}^2) &:= \{v \in P_1(\mathcal{T}; \mathbb{R}^2) : \forall E \in \mathcal{E}, v \text{ is continuous at } \text{mid}(E)\}, \\ \text{CR}_0^1(\mathcal{T}; \mathbb{R}^2) &:= \{v \in \text{CR}^1(\mathcal{T}; \mathbb{R}^2) : \forall E \in \mathcal{E}(\partial\Omega), v(\text{mid}(E)) = 0\}. \end{aligned}$$

The Crouzeix-Raviart finite element functions form a subspace of the piecewise Sobolev functions

$$H^1(\mathcal{T}; \mathbb{R}^2) := \{v \in L^2(\Omega; \mathbb{R}^2) : \forall T \in \mathcal{T}, v|_T \in H^1(T; \mathbb{R}^2) := H^1(\text{int}(T); \mathbb{R}^2)\}.$$

The corresponding piecewise differential operators $\text{D}_{\text{NC}} : H^1(\mathcal{T}; \mathbb{R}^2) \rightarrow L^2(\Omega; \mathbb{R}^{2 \times 2})$ and $\text{div}_{\text{NC}} : H^1(\mathcal{T}; \mathbb{R}^2) \rightarrow L^2(\Omega)$ read, for $v \in H^1(\mathcal{T}; \mathbb{R}^2)$,

$$(\text{D}_{\text{NC}} v)|_T := \text{D}(v|_T) \quad \text{and} \quad (\text{div}_{\text{NC}} v)|_T := \text{div}(v|_T) \quad \text{for all } T \in \mathcal{T}.$$

The integral mean of a function $f \in L^2(\omega)$ (or any vector $f \in L^2(\omega; \mathbb{R}^2)$) over some set ω is

$$f_\omega := \int_\omega f \, dx := \int_\omega f \, dx / |\omega|.$$

Given $f \in L^2(\Omega)$ (as well as vectors $f \in L^2(\Omega; \mathbb{R}^2)$), let $f_{\mathcal{T}} := \Pi f$ denote the L^2 -orthogonal projection of f onto the piecewise constant functions $P_0(\mathcal{T})$ (resp. $P_0(\mathcal{T}; \mathbb{R}^2)$) and

$$\text{osc}^2(f, \mathcal{T}) := \sum_{T \in \mathcal{T}} \text{osc}^2(f, T) = \|h_{\mathcal{T}}(f - f_{\mathcal{T}})\|_{L^2(\Omega)}^2 \quad \text{with} \quad \text{osc}^2(f, T) := \|h_T(f - f_T)\|_{L^2(T)}^2.$$

For given $f \in L^2(\Omega; \mathbb{R}^2)$, let the right-hand side functional be

$$F(v) := \int_\Omega f \cdot v \, dx \quad \text{for all } v \in H^1(\mathcal{T}; \mathbb{R}^2). \tag{2.1}$$

C. Crouzeix-Raviart FEM for the Stokes Equations

The first discrete bilinear form reads

$$a_{\text{NC}}(u_{\text{CR}}, v_{\text{CR}}) := \sum_{T \in \mathcal{T}} \int_T \text{D}u_{\text{CR}} : \text{D}v_{\text{CR}} \, dx$$

for all $u_{\text{CR}}, v_{\text{CR}} \in \text{CR}^1(\mathcal{T}; \mathbb{R}^2) \subseteq H^1(\mathcal{T}; \mathbb{R}^2)$ with $A : B := \sum_{j,k=1,2} A_{jk} B_{jk}$ for all 2×2 matrices $A, B \in \mathbb{R}^{2 \times 2}$. Let $L_0^2(\Omega) := \{q \in L^2(\Omega) : \int_{\Omega} q \, dx = 0\}$ denote the space of L^2 functions with zero integral mean. Then, the second discrete bilinear form reads

$$b_{\text{NC}}(v_{\text{CR}}, q_0) := \int_{\Omega} q_0 \operatorname{div}_{\text{NC}} v_{\text{CR}} \, dx$$

for all $v_{\text{CR}} \in \text{CR}_0^1(\mathcal{T}; \mathbb{R}^2)$ and $q_0 \in P_0(\mathcal{T}) \cap L_0^2(\Omega)$. This leads to the discrete counterpart

$$Z_{\text{NC}} := \{v_{\text{CR}} \in \text{CR}_0^1(\mathcal{T}; \mathbb{R}^2) : \operatorname{div}_{\text{NC}} v_{\text{CR}} = 0 \text{ a.e. in } \Omega\}$$

of the set of divergence-free functions

$$Z := \{v \in H_0^1(\Omega; \mathbb{R}^2) : \operatorname{div} v = 0 \text{ a.e. in } \Omega\}.$$

The nonconforming representation of the Stokes problem reads: Given $f \in L^2(\Omega; \mathbb{R}^2)$ and $u_D \in L^2(\Omega; \mathbb{R}^2)$ with $\int_{\partial\Omega} u_D \cdot \nu \, ds = 0$, seek $u_{\text{CR}} \in Z_{\text{NC}}$ with

$$u_{\text{CR}}(\operatorname{mid}(E)) = \int_E u_D \, ds \quad \text{for all } E \in \mathcal{E}(\partial\Omega) \quad \text{and}$$

$$a_{\text{NC}}(u_{\text{CR}}, v_{\text{CR}}) = F(v_{\text{CR}}) \quad \text{for all } v_{\text{CR}} \in Z_{\text{NC}}.$$

In other words, up to boundary conditions, u_{CR} is computed from the Riesz representation of a linear functional (given as right-hand side plus boundary modifications) in the Hilbert space $(Z_{\text{NC}}, a_{\text{NC}})$. The actual implementation uses unconstrained Crouzeix-Raviart elements $v_{\text{CR}} \in \text{CR}_0^1(\mathcal{T}; \mathbb{R}^2)$ as test functions and enforce the constraint $\operatorname{div}_{\text{NC}} u_{\text{CR}} = 0$ a.e. in Ω by piecewise constant Lagrange multipliers in $P_0(\mathcal{T}) \cap L_0^2(\Omega)$. Hence, u_{CR} from above and some $p_{\text{CR}} \in P_0(\mathcal{T}) \cap L_0^2(\Omega)$ are determined by

$$a_{\text{NC}}(u_{\text{CR}}, v_{\text{CR}}) + b_{\text{NC}}(v_{\text{CR}}, p_{\text{CR}}) = F(v_{\text{CR}}) \quad \text{for all } v_{\text{CR}} \in \text{CR}_0^1(\mathcal{T}; \mathbb{R}^2),$$

$$b_{\text{NC}}(u_{\text{CR}}, q_{\text{CR}}) = 0 \quad \text{for all } q_{\text{CR}} \in P_0(\mathcal{T}) \cap L_0^2(\Omega).$$

III. PSEUDOSTRESS APPROXIMATION AND ERROR ANALYSIS

A simple postprocessing of the Crouzeix-Raviart nonconforming solution $\hat{u}_{\text{CR}} \in Z_{\text{NC}}$ and $\hat{p}_{\text{CR}} \in P_0(\mathcal{T}) \cap L_0^2(\Omega)$ with respect to the piecewise constant right-hand side $f_{\mathcal{T}}$ (instead of f in (2.1)) leads to the pseudostress representation

$$\sigma_{\text{PS}} := D_{\text{NC}} \hat{u}_{\text{CR}} - \frac{f_{\mathcal{T}}}{2} \otimes (\bullet - \operatorname{mid}(\mathcal{T})) - \hat{p}_{\text{CR}} I_{2 \times 2} \quad \text{and}$$

$$u_{\text{PS}} := \Pi \hat{u}_{\text{CR}} + \frac{1}{4} \Pi(\operatorname{dev}(f_{\mathcal{T}} \otimes (\bullet - \operatorname{mid}(\mathcal{T}))) (\bullet - \operatorname{mid}(\mathcal{T}))),$$

where $\operatorname{mid}(\mathcal{T})$ denotes the piecewise constant vector-valued function with $\operatorname{mid}(\mathcal{T})|_T := \operatorname{mid}(T)$ and $\operatorname{dev}(A) := A - \operatorname{tr}(A) I_{2 \times 2} / 2$ denotes the deviatoric part of some matrix-valued function A . Then, the piecewise quadratic function

$$u_2 := \hat{u}_{\text{CR}} - \frac{f_{\mathcal{T}}}{4} (|\bullet - \operatorname{mid}(\mathcal{T})|^2 - \|\bullet - \operatorname{mid}(\mathcal{T})\|_{L^2(\Omega)}^2) \in P_2(\mathcal{T}; \mathbb{R}^2)$$

satisfies $D_{\text{NC}} u_2 = \sigma_{\text{PS}} + \hat{p}_{\text{CR}} I_{2 \times 2}$.

The pair (σ_{PS}, u_{PS}) solves the Raviart-Thomas mixed FEM [4, 3] with respect to f and approximates the exact pseudostress

$$\sigma = Du - pI_{2 \times 2} \in H(\operatorname{div}, \Omega; \mathbb{R}^{2 \times 2})/\mathbb{R} := \left\{ \tau \in H(\operatorname{div}, \Omega; \mathbb{R}^{2 \times 2}) : \int_{\Omega} \operatorname{tr} \tau \, dx = 0 \right\}$$

with $f + \operatorname{div} \sigma = 0$ and the exact solution $u \in H^1(\Omega; \mathbb{R}^2)$ in the discrete spaces

$$\operatorname{PS}(\mathcal{T}) := \left\{ \tau \in P_1(\mathcal{T}; \mathbb{R}^{2 \times 2}) \cap H(\operatorname{div}, \Omega; \mathbb{R}^{2 \times 2})/\mathbb{R} : \forall j = 1, 2, (\tau_{j1}, \tau_{j2}) \in \operatorname{RT}_0(\mathcal{T}) \right\}$$

and $P_0(\mathcal{T}; \mathbb{R}^2)$ such that $f_{\mathcal{T}} + \operatorname{div} \sigma_{PS} = 0$ a.e. in Ω . In fact, the following discrete formulation has the unique solution $(\sigma_{PS}, u_{PS}) \in \operatorname{PS}(\mathcal{T}) \times P_0(\mathcal{T}; \mathbb{R}^2)$,

$$\int_{\Omega} \operatorname{dev} \sigma_{PS} : \tau_{PS} \, dx + \int_{\Omega} \operatorname{div} \tau_{PS} \cdot u_{PS} \, dx = \int_{\partial\Omega} u_D \cdot \tau_{PS} \nu \, ds \text{ for all } \tau_{PS} \in \operatorname{PS}(\mathcal{T}), \tag{3.1}$$

$$\int_{\Omega} \operatorname{div} \sigma_{PS} \cdot v_{PS} \, dx = - \int_{\Omega} f \cdot v_{PS} \, dx \text{ for all } v_{PS} \in P_0(\mathcal{T}; \mathbb{R}^2). \tag{3.2}$$

The following theorem recalls the known results for the Crouzeix-Raviart finite element method from [13, 8] for the pseudostress-related approximation u_2 with the set of admissible test functions $\mathcal{A} := \{v \in H^1(\Omega; \mathbb{R}^2) : v = u_D \text{ on } \partial\Omega\}$. Moreover, a refined guaranteed upper bound that follows an idea from [9] is introduced. This idea is based on a partition of Ω into J many subdomains $\Omega_1, \dots, \Omega_J$ with $\cup_{j=1}^J \overline{\Omega}_j = \overline{\Omega}$, outer unit normal vectors ν_{Ω_j} and local inf-sup constants

$$0 < c_j := \inf_{q \in L^2_0(\Omega_j) \setminus \{0\}} \sup_{v \in H^1_0(\Omega_j; \mathbb{R}^2) \setminus \{0\}} \int_{\Omega_j} q \operatorname{div} v \, dx / (\|D v\|_{L^2(\Omega_j)} \|q\|_{L^2(\Omega_j)}) \text{ for } j = 1, \dots, J.$$

The set of test functions that are suitable for the refined error control satisfy an additional constraint and are defined by

$$\tilde{\mathcal{A}} := \left\{ v \in \mathcal{A} : \int_{\partial\Omega_j} v \cdot \nu_{\Omega_j} \, ds = 0 \text{ for } j = 1, \dots, J \right\}. \tag{3.3}$$

Moreover, the constant $j_{1,1} \geq 3.8317$ below denotes the first positive root of the first Bessel function.

Theorem 3.1.

(a) Any $v \in \mathcal{A}$ satisfies

$$\| \|u - u_2\|_{NC}^2 \leq \operatorname{osc}(f, \mathcal{T})^2 / j_{1,1}^2 + (\|v - u_2\|_{NC} + \|\operatorname{div} v\|_{L^2(\Omega)} / c_0)^2.$$

(b) Any $v \in \tilde{\mathcal{A}}$ from (3.3) satisfies

$$\| \|u - u_2\|_{NC}^2 \leq \operatorname{osc}(f, \mathcal{T})^2 / j_{1,1}^2 + \sum_{j=1}^J (\|D_{NC}(v - u_2)\|_{L^2(\Omega_j)} + \|\operatorname{div} v\|_{L^2(\Omega_j)} / c_j)^2.$$

Proof of Theorem 3.1(a). The point of departure is the orthogonal split from [8, Subsection 3.2],

$$D_{\text{NC}}(u - u_2) = Dz + y \tag{3.4}$$

into some $z \in Z$ with

$$\int_{\Omega} Dz : Dv \, dx = \int_{\Omega} D_{\text{NC}}(u - u_2) : Dv \, dx \quad \text{for all } v \in Z$$

and the remainder

$$y \in Y := \left\{ y \in L^2(\Omega; \mathbb{R}^{2 \times 2}) : \int_{\Omega} y : Dv \, dx = 0 \text{ for all } v \in Z \right\}.$$

Since Y is the orthogonal complement of $D(Z)$ in $L^2(\Omega; \mathbb{R}^{2 \times 2})$, it follows

$$\| \|u - u_2\|_{\text{NC}}^2 = \| \|z\|^2 + \|y\|_{L^2(\Omega)}^2. \tag{3.5}$$

Since $z \in Z$, $I_{2 \times 2} : Dz = \text{div } z = 0$ a.e. This, the aforementioned orthogonality, and an integration by parts show

$$\begin{aligned} \| \|z\|^2 &= \int_{\Omega} D_{\text{NC}}(u - u_2) : Dz \, dx = \int_{\Omega} Du : Dz \, dx - \int_{\Omega} D_{\text{NC}}u_2 : Dz \, dx \\ &= \int_{\Omega} f \cdot z \, dx - \int_{\Omega} \sigma_{\text{PS}} : Dz \, dx = \int_{\Omega} f \cdot z \, dx + \int_{\Omega} z \cdot \text{div } \sigma_{\text{PS}} \, dx = \int_{\Omega} (f - f_T) \cdot z \, dx. \end{aligned}$$

Piecewise Poincaré inequalities (with Poincaré constant $h_T/j_{1,1}$ from [20, Corollary 3.4]) then imply

$$\begin{aligned} \int_{\Omega} (f - f_T) \cdot z \, dx &= \int_{\Omega} (f - f_T) \cdot (z - z_T) \, dx \leq \sum_{T \in \mathcal{T}} \|f - f_T\|_{L^2(T)} \|z - z_T\|_{L^2(T)} \\ &\leq \sum_{T \in \mathcal{T}} h_T/j_{1,1} \|f - f_T\|_{L^2(T)} \|Dz\|_{L^2(T)} \leq \text{osc}(f, \mathcal{T})/j_{1,1} \| \|z\|. \end{aligned}$$

Hence,

$$\| \|z\| \leq \text{osc}(f, \mathcal{T})/j_{1,1}. \tag{3.6}$$

For each $y \in Y$, there exists some $q \in L^2_0(\Omega)$ [8, Subsection 3.2, Lemma 2] with

$$\int_{\Omega} y : Dw \, dx = \int_{\Omega} q \, \text{div } w \, dx \quad \text{for all } w \in H^1_0(\Omega; \mathbb{R}^2) \quad \text{and} \quad c_0 \|q\|_{L^2(\Omega)} \leq \|y\|_{L^2(\Omega)}.$$

Hence, any $v \in \mathcal{A}$ with $u - v = 0$ on $\partial\Omega$ satisfies

$$\begin{aligned} \|y\|_{L^2(\Omega)}^2 &= \int_{\Omega} D_{\text{NC}}(u - u_2) : y \, dx = \int_{\Omega} D_{\text{NC}}(v - u_2) : y \, dx + \int_{\Omega} D(u - v) : y \, dx \\ &= \int_{\Omega} D_{\text{NC}}(v - u_2) : y \, dx + \int_{\Omega} q \, \text{div } (u - v) \, dx \\ &\leq (\|D_{\text{NC}}(v - u_2)\|_{L^2(\Omega)} + \|\text{div } v\|_{L^2(\Omega)}/c_0) \|y\|_{L^2(\Omega)}. \end{aligned}$$

Therefore,

$$\|y\|_{L^2(\Omega)} \leq \|D_{\text{NC}}(v - u_2)\|_{L^2(\Omega)} + \|\operatorname{div} v\|_{L^2(\Omega)}/c_0. \tag{3.7}$$

The combination of (3.5)–(3.7) concludes the proof. ■

Proof of Theorem 3.1(b). The proof follows ideas from [9] for the local versions

$$Z_j := \{z \in H_0^1(\Omega_j; \mathbb{R}^2) : \operatorname{div} z = 0 \text{ a.e. in } \Omega_j\} \quad \text{and}$$

$$Y_j := \left\{ y \in L^2(\Omega_j; \mathbb{R}^{2 \times 2}) : \int_{\Omega_j} y : Dz \, dx = 0 \text{ for all } z \in Z_j \right\}$$

of Z and Y from the proof of (a) with Ω replaced by Ω_j .

Given $v \in \tilde{\mathcal{A}}$ and any $j = 1, \dots, J$, the condition $\int_{\partial\Omega_j} v \cdot \nu_j \, ds = 0$ guarantees that the Stokes equations with volume force f_T has a unique solution $w_j \in Z_j$ with the boundary data $w_j = v$ along $\partial\Omega_j$, i.e.,

$$\int_{\Omega_j} Dw_j : D\zeta_j \, dx = \int_{\Omega_j} f_T \cdot \zeta_j \, dx \quad \text{for all } \zeta_j \in Z_j. \tag{3.8}$$

Furthermore, there exist $z_j \in Z_j$ and $y_j \in Y_j$ with

$$D_{\text{NC}}(w_j - u_2) = Dz_j + y_j \quad \text{on } \Omega_j.$$

Since Y_j is the orthogonal complement of $D(Z_j)$ in $L^2(\Omega_j; \mathbb{R}^{2 \times 2})$, it follows

$$\|D_{\text{NC}}(w_j - u_2)\|_{L^2(\Omega_j)}^2 = \|Dz_j\|_{L^2(\Omega_j)}^2 + \|y_j\|_{L^2(\Omega_j)}^2. \tag{3.9}$$

The combination of the aforementioned orthogonality with (3.8), $\operatorname{div} z_j = 0$ a.e. in Ω_j , $\operatorname{dev} \sigma_{\text{PS}} = \operatorname{dev} D_{\text{NC}}u_2$ and $f_T + \operatorname{div} \sigma_{\text{PS}} = 0$ yields

$$\begin{aligned} \|Dz_j\|_{L^2(\Omega_j)}^2 &= \int_{\Omega_j} D_{\text{NC}}(w_j - u_2) : Dz_j \, dx = \int_{\Omega_j} Dw_j : Dz_j \, dx - \int_{\Omega_j} D_{\text{NC}}u_2 : Dz_j \, dx \\ &= \int_{\Omega_j} f_T \cdot z_j \, dx - \int_{\Omega_j} \sigma_{\text{PS}} : Dz_j \, dx = \int_{\Omega_j} (f_T + \operatorname{div} \sigma_{\text{PS}}) \cdot z_j \, dx = 0. \end{aligned} \tag{3.10}$$

For each $y_j \in Y_j$, there exists some $q_j \in L_0^2(\Omega_j)$ [8, Subsection 3.2, Lemma 2] with

$$\int_{\Omega_j} y_j : D\varphi_j \, dx = \int_{\Omega_j} q_j \operatorname{div} \varphi_j \, dx \quad \text{for all } \varphi_j \in H_0^1(\Omega_j; \mathbb{R}^2) \quad \text{and}$$

$$c_j \|q_j\|_{L^2(\Omega_j)} \leq \|y_j\|_{L^2(\Omega_j)}.$$

The combination of this result for the test function $\varphi_j \equiv w_j - v \in H_0^1(\Omega_j; \mathbb{R}^2)$ with the aforementioned orthogonality and a Cauchy inequality result in

$$\begin{aligned} \|y_j\|_{L^2(\Omega_j)}^2 &= \int_{\Omega_j} y_j : D_{\text{NC}}(w_j - u_2) \, dx = \int_{\Omega_j} y_j : D_{\text{NC}}(v - u_2) \, dx + \int_{\Omega_j} y_j : D_{\text{NC}}(w_j - v) \, dx \\ &\leq (\|D_{\text{NC}}(v - u_2)\|_{L^2(\Omega_j)} + \|\operatorname{div} \varphi_j\|_{L^2(\Omega_j)}/c_j) \|y_j\|_{L^2(\Omega_j)}. \end{aligned}$$

This, (3.9), (3.10), and $\operatorname{div} w_j = 0$ a.e. in Ω_j imply, for $j = 1, \dots, J$,

$$\|D_{\text{NC}}(w_j - u_2)\|_{L^2(\Omega_j)} = \|y_j\|_{L^2(\Omega_j)} \leq \|D_{\text{NC}}(v - u_2)\|_{L^2(\Omega_j)} + \|\operatorname{div} v\|_{L^2(\Omega_j)}/c_j. \tag{3.11}$$

The functions $w_j, z_j \in H_0^1(\Omega_j; \mathbb{R}^2)$ can be extended by zero to $\tilde{w}_j, \tilde{z}_j \in H_0^1(\Omega; \mathbb{R}^2)$ (i.e. $\tilde{w}_j := w_j$ and $\tilde{z}_j := z_j$ in Ω_j and $\tilde{w}_j, \tilde{z}_j := 0$ in $\Omega \setminus \Omega_j$) and $y_j \in L^2(\Omega_j; \mathbb{R}^{2 \times 2})$ can be extended by zero to $\tilde{y}_j \in L^2(\Omega; \mathbb{R}^{2 \times 2})$ (i.e. $\tilde{y}_j := y_j$ in Ω_j and $\tilde{y}_j := 0$ in $\Omega \setminus \Omega_j$). Then the sums $\tilde{z} := \tilde{z}_1 + \dots + \tilde{z}_J$ and $\tilde{w} := \tilde{w}_1 + \dots + \tilde{w}_J$ belong to Z .

Since $\operatorname{div} \tilde{w} = 0$ a.e. in Ω , part (a) proves for $\tilde{w} \in \mathcal{A}$ that

$$\|u - u_2\|_{\text{NC}}^2 \leq \operatorname{osc}(f, \mathcal{T})^2 / j_{1,1}^2 + \|\tilde{w} - u_2\|_{\text{NC}}^2.$$

The estimate (3.11) implies

$$\|\tilde{w} - u_2\|_{\text{NC}}^2 = \sum_{j=1}^J \|D_{\text{NC}}(w_j - u_2)\|_{L^2(\Omega_j)}^2 \leq \sum_{j=1}^J (\|D_{\text{NC}}(v - u_2)\|_{L^2(\Omega_j)} + \|\operatorname{div} v\|_{L^2(\Omega_j)}/c_j)^2.$$

This concludes the proof of (b). ■

IV. PROPER INTERPOLATION DESIGNS

This section designs functions $v \in \mathcal{A}$ with the additional prerequisites

$$\int_{\partial\Omega_j} v \cdot \nu_{\Omega_j} \, ds = 0 \quad \text{for } j = 1, \dots, J \tag{4.1}$$

for Theorem 3.1 (b) by modifications of the designs compared in [13]. All designs satisfy a discrete Dirichlet boundary condition of the set of admissible functions defined by

$$\begin{aligned} \mathcal{A}(\mathcal{T}) &:= \{v \in C(\overline{\Omega}; \mathbb{R}^2) : v(z) = u_D(z) \text{ for all } z \in \mathcal{N}(\partial\Omega)\} \quad \text{and} \\ \tilde{\mathcal{A}}(\mathcal{T}) &:= \{v \in \mathcal{A}(\mathcal{T}) : v \text{ satisfies (4.1)}\}. \end{aligned}$$

These functions violate the exact Dirichlet boundary condition, see Subsection IV.D for a remedy. Furthermore, $\mathcal{E}(\Gamma) := \{E \in \mathcal{E} : E \subseteq \Gamma\}$ defines the set of edges along the skeleton $\Gamma := \cup_{j=1}^J \partial\Omega_j$.

A. Piecewise Quadratic Interpolation

A nodal averaging of u_2 as in [13] leads to the piecewise quadratic and continuous function $v_{\text{AP2}} \in P_2(\mathcal{T}; \mathbb{R}^2) \cap \tilde{\mathcal{A}}(\mathcal{T})$, defined via piecewise quadratic interpolation of the values at the nodes $z \in \mathcal{N}$

$$v_{\text{AP2}}(z) := \begin{cases} u_D(z) & \text{for } z \in \mathcal{N}(\partial\Omega), \\ \sum_{T \in \mathcal{T}(z)} u_2|_T(z) / |T(z)| & \text{for } z \in \mathcal{N}(\Omega), \end{cases}$$

and in the midpoints of the edges $E \in \mathcal{E}$ with the two adjacent triangles $\mathcal{T}(\text{mid}(E))$ of $E \in \mathcal{E}(\Omega)$ and the two endpoints $\mathcal{N}(E)$

$$v_{\text{AP2}}(\text{mid}(E)) := \begin{cases} \sum_{T \in \mathcal{T}(\text{mid}(E))} u_2|_T / |\mathcal{T}(\text{mid}(E))| & \text{for } E \in \mathcal{E}(\Omega) \setminus \mathcal{E}(\Gamma), \\ 3\hat{u}_{\text{CR}}(\text{mid}(E))/2 - \sum_{z \in \mathcal{N}(E)} v_{\text{AP2}}(z)/4 & \text{for } E \in \mathcal{E}(\Gamma). \end{cases}$$

Let $(\varphi_z : z \in \mathcal{N} \cup \text{mid}(\mathcal{E}))$ denote the piecewise quadratic and globally continuous basis functions of $P_2(\mathcal{T}) \cap C(\bar{\Omega})$. The definition of v_{AP2} implies

$$\begin{aligned} \int_{\partial\Omega_j} v_{\text{AP2}} \cdot \nu \, ds &= \sum_{E \in \mathcal{E}(\partial\Omega_j)} \int_E v_{\text{AP2}} \cdot \nu \, ds \\ &= \sum_{E \in \mathcal{E}(\partial\Omega_j)} \left(v_{\text{AP2}}(\text{mid}(E)) \int_E \varphi_{\text{mid}(E)} \, ds + \sum_{z \in \mathcal{N}(E)} v_{\text{AP2}}(z) \int_E \varphi_z \, ds \right) \cdot \nu_{\Omega_j}|_E \\ &= \sum_{E \in \mathcal{E}(\partial\Omega_j)} |E|/6 \left(4v_{\text{AP2}}(\text{mid}(E)) + \sum_{z \in \mathcal{N}(E)} v_{\text{AP2}}(z) \right) \cdot \nu_{\Omega_j}|_E \\ &= \sum_{E \in \mathcal{E}(\partial\Omega_j)} |E| \hat{u}_{\text{CR}}(\text{mid}(E)) \cdot \nu_{\Omega_j}|_E = \int_{\partial\Omega_j} \hat{u}_{\text{CR}} \cdot \nu_{\Omega_j} \, ds = \int_{\Omega_j} \text{div}_{\text{NC}} \hat{u}_{\text{CR}} \, dx = 0. \end{aligned}$$

Hence, $v \equiv v_{\text{AP2}}$ satisfies condition (4.1).

B. Minimal Piecewise Quadratic Interpolation

A global minimization of the guaranteed upper bound from Theorem 3.1 (b) leads to

$$\begin{aligned} v_{\text{MP2}} &:= \operatorname{argmin}_{v \in P_2(\mathcal{T}; \mathbb{R}^2) \cap \tilde{\mathcal{A}}(\mathcal{T})} \sum_{j=1}^J (\|D_{\text{NC}}(v - u_2)\|_{L^2(\Omega_j)} + \|\operatorname{div} v\|_{L^2(\Omega_j)}/c_j)^2 \\ &= \operatorname{argmin}_{v \in P_2(\mathcal{T}; \mathbb{R}^2) \cap \tilde{\mathcal{A}}(\mathcal{T})} \sum_{j=1}^J \min_{0 < \mu_j < \infty} ((1 + \mu_j) \|D_{\text{NC}}(v - u_2)\|_{L^2(\Omega_j)}^2 \\ &\quad + (1 + 1/\mu_j) \|\operatorname{div} v\|_{L^2(\Omega_j)}/c_j^2) \end{aligned}$$

and is realized by the following algorithm.

Algorithm 4.1 (global minimization).

Input $\hat{u}_2 \in P_2(\mathcal{T}; \mathbb{R}^2)$, $c_1, \dots, c_j, \Omega_1, \dots, \Omega_J$ and the number of iterations $K \in \mathbb{N}$.

Initialize $\mu_j := 1$ for $j = 1, \dots, J$.

for $k = 1, \dots, K$ **do**

Compute $v_{\text{MP2}(k)} :=$

$$\operatorname{argmin}_{v \in P_2(\mathcal{T}; \mathbb{R}^2) \cap \tilde{\mathcal{A}}(\mathcal{T})} \sum_{j=1}^J ((1 + \mu_j) \|D_{\text{NC}}(v - u_2)\|_{L^2(\Omega_j)}^2 + (1 + 1/\mu_j) \|\operatorname{div} v\|_{L^2(\Omega_j)}/c_j^2),$$

$\mu_j := \|\operatorname{div} v_{\text{MP2}(k)}\|_{L^2(\Omega_j)}/(c_j \|D_{\text{NC}}(v_{\text{MP2}(k)} - u_2)\|_{L^2(\Omega_j)})$ for $j = 1, \dots, J$. **od**

Output $v_{\text{MP2}(K)} \in P_2(\mathcal{T}; \mathbb{R}^2) \cap \tilde{\mathcal{A}}(\mathcal{T})$.

The condition (4.1) (involved in $\tilde{\mathcal{A}}(\mathcal{T})$) may be enforced by Lagrange multipliers $\lambda \in \mathbb{R}^J$. The computation of $v_{\text{MP2}(k)}$ requires a solution of a linear system in each step. In order to reduce the computational costs, we use three iterations of a preconditioned conjugate gradient method for inexact solve and denote the solution with $v_{\text{MP2CG3}(K)}$. The preconditioner is the diagonal of the system matrix named after Jacobi. Note that this solution might not satisfy condition (4.1) exactly. For a remedy, the reader is referred to Subsection IV.E.

Undisplayed numerical experiments show that the values after $K=3$ iterations do not significantly change anymore.

C. Piecewise Linear Interpolation on Red-Refinement

This subsection designs piecewise linear $v_{\text{red}} \in P_1(\text{red}(\mathcal{T}); \mathbb{R}^2) \cap \tilde{\mathcal{A}}(\mathcal{T})$ with respect to the uniform red-refinement $\text{red}(\mathcal{T})$ of triangulation \mathcal{T} [7, 13]. The nodes of $\text{red}(\mathcal{T})$ consists of the nodes \mathcal{N} and the edge midpoints $\text{mid}(\mathcal{E})$ of \mathcal{T} . Define $v_{\text{red}} \in P_1(\text{red}(\mathcal{T}); \mathbb{R}^2) \cap \tilde{\mathcal{A}}(\mathcal{T})$ via piecewise linear interpolation of the values, for the node $z \in \mathcal{N}$,

$$v_{\text{red}}(z) := \begin{cases} u_D(z) & \text{for } z \in \mathcal{N}(\partial\Omega), \\ v_z & \text{for } z \in \mathcal{N}(\Omega) \end{cases} \tag{4.2}$$

with some particular choice of $v_z \in \mathbb{R}^2$, and in the midpoints of the edges $E \in \mathcal{E}$,

$$v_{\text{red}}(\text{mid}(E)) := \begin{cases} \hat{u}_{\text{CR}}(\text{mid}(E)) & \text{for } E \in \mathcal{E}(\Omega) \setminus \mathcal{E}(\Gamma), \\ 2\hat{u}_{\text{CR}}(\text{mid}(E)) - \sum_{z \in \mathcal{N}(E)} v_{\text{red}}(z)/2 & \text{for } E \in \mathcal{E}(\Gamma). \end{cases} \tag{4.3}$$

Define $(\varphi_z^{\text{red}} : z \in \mathcal{N} \cup \text{mid}(\mathcal{E}))$ as the nodal basis functions in $P_1(\text{red}(\mathcal{T})) \cap C(\bar{\Omega})$. The definition of v_{red} implies

$$\begin{aligned} \int_{\partial\Omega_j} v_{\text{red}} \cdot \nu \, ds &= \sum_{E \in \mathcal{E}(\partial\Omega_j)} \int_E v_{\text{red}} \cdot \nu \, ds \\ &= \sum_{E \in \mathcal{E}(\partial\Omega_j)} \left(v_{\text{red}}(\text{mid}(E)) \int_E \varphi_{\text{mid}(E)}^{\text{red}} \, ds + \sum_{z \in \mathcal{N}(E)} v_{\text{red}}(z) \int_E \varphi_z^{\text{red}} \, ds \right) \cdot \nu_{\Omega_j}|_E \\ &= \sum_{E \in \mathcal{E}(\partial\Omega_j)} |E|/4 \left(2v_{\text{red}}(\text{mid}(E)) + \sum_{z \in \mathcal{N}(E)} v_{\text{red}}(z) \right) \cdot \nu_{\Omega_j}|_E \\ &= \sum_{E \in \mathcal{E}(\partial\Omega_j)} |E| \hat{u}_{\text{CR}}(\text{mid}(E)) \cdot \nu_{\Omega_j}|_E = \int_{\partial\Omega_j} \hat{u}_{\text{CR}} \cdot \nu_{\Omega_j} \, ds = \int_{\Omega_j} \text{div } \hat{u}_{\text{CR}} \, dx = 0. \end{aligned}$$

Hence, $v \equiv v_{\text{red}}$ satisfies condition (4.1).

Interpolation v_{red} is fixed on all central subtriangles as T_4 in Fig. 1(b) and it remains to determine the values v_z at the free nodes $z \in \mathcal{N}(\Omega)$, e.g. by nodal averaging

$$v_z := \sum_{T \in \mathcal{T}(z)} \hat{u}_{\text{CR}}|_T(z)/|\mathcal{T}(z)| \quad \text{for all } z \in \mathcal{N}(\Omega). \tag{4.4}$$

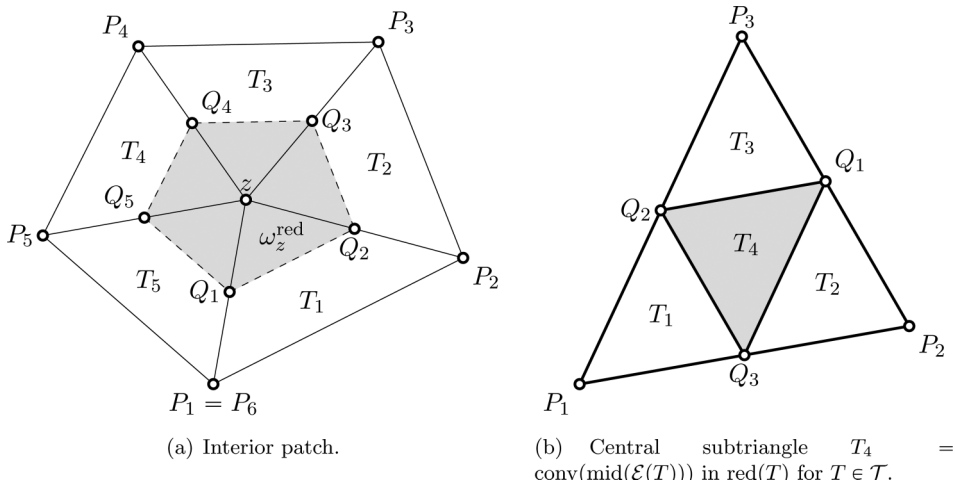


FIG. 1. Notation for red-refinements.

Algorithm 4.2 below suggests the one-dimensional minimization problem around each node patch ω_z^{red} with respect to the red-refined triangulation as in Fig. 1(a) under the side condition of the fixed values at the edge midpoints Q_j of the adjacent edges.

Algorithm 4.2 (patchwise minimization).

Input $\hat{u}_{CR} \in C^1(\mathcal{T}; \mathbb{R}^2)$, $c_1, \dots, c_J, \Omega_1, \dots, \Omega_J$ and the number of iterations $K \in \mathbb{N}$.

Initialize $v_{PMred} := \sum_{E \in \mathcal{E}} \hat{u}_{CR}(\text{mid}(E)) \varphi_{\text{mid}(E)}^{\text{red}}$ and $\mu_j := 1$ for $j = 1, \dots, J$.

for $k = 1, \dots, K$ **do**

$v_0 := \sum_{E \in \mathcal{E}} v_{PMred}(\text{mid}(E)) \varphi_{\text{mid}(E)}^{\text{red}}$,
 $\forall z \in \mathcal{N}(\Omega)$ **compute**

$$v_z := \underset{w \in \mathbb{R}^2}{\text{argmin}} \sum_{j=1}^J ((1 + \mu_j) \|D_{NC}(v_0 + w \varphi_z^{\text{red}} - u_2)\|_{L^2(\omega_z^{\text{red}} \cap \Omega_j)}^2 + (1 + 1/\mu_j)/c_j^2 \|\text{div}(v_0 + w \varphi_z^{\text{red}})\|_{L^2(\omega_z^{\text{red}} \cap \Omega_j)}^2),$$

$v_{PMred} := v_0 + \sum_{z \in \mathcal{N}(\Omega)} v_z \varphi_z^{\text{red}}$,
 $\forall j = 1, \dots, J$ **compute** $\mu_j := \|\text{div} v_{PMred}\|_{L^2(\Omega_j)} / (c_j \|D_{NC}(v_{PMred} - u_2)\|_{L^2(\Omega_j)})$. *od*

Output $v_{PMred} \in P_1(\text{red}(\mathcal{T}); \mathbb{R}^2) \cap \tilde{\mathcal{A}}(\mathcal{T})$.

Undisplayed numerical experiments show that the values after $K=3$ iterations do not significantly change anymore.

We distinguish between the optimal version v_{PMred} from Algorithm 4.2, and v_{MAred} with the suboptimal choice v_z from (4.4).

D. Inhomogeneous Dirichlet Boundary Conditions

In case of inhomogeneous Dirichlet boundary conditions all designs in Subsections IV.A–IV.C result in some v_{xyz} which does not necessarily belong to \mathcal{A} . To overcome this shortcoming, a virtual boundary reconstruction $w_D \in H^1(\Omega)$ with $w_D = u_D - v_{xyz}$ along $\partial\Omega$ as in [21, 7, 13]

allows $v := v_{xyz} + w_D \in \mathcal{A}$ and the estimates

$$\begin{aligned} \|\mathbf{D}_{\text{NC}}(v - u_2)\|_{L^2(\Omega_j)} + \|\operatorname{div} v\|_{L^2(\Omega_j)}/c_j &\leq \|\mathbf{D}_{\text{NC}}(v_{xyz} - u_2)\|_{L^2(\Omega_j)} + \|\operatorname{div} v_{xyz}\|_{L^2(\Omega_j)}/c_j \\ &\quad + \|\mathbf{D}w_D\|_{L^2(\Omega_j)} + \|\operatorname{div} w_D\|_{L^2(\Omega_j)}/c_j. \end{aligned}$$

The divergence and energy norm of w_D can be estimated by [21, Theorem 4.2]

$$\|\operatorname{div} w_D\|_{L^2(\Omega_j)} \leq \sqrt{2} \|\mathbf{D}w_D\|_{L^2(\Omega_j)} \leq \sqrt{2} C_\gamma \|h_\mathcal{E}^{3/2} \partial_\mathcal{E}^2 (u_D - v_{xyz})/\partial s^2\|_{L^2(\partial\Omega_j \cap \partial\Omega)}.$$

The construction of w_D ensures $\int_E w_D \, ds = 0$ for all $E \in \mathcal{E}(\partial\Omega_j)$. Hence, $v \equiv v_{xyz} + w_D \in \tilde{\mathcal{A}}(\mathcal{T})$ for any $v_{xyz} \in \tilde{\mathcal{A}}(\mathcal{T})$.

For right isosceles triangles, numerical calculations in [7] suggest the constant $C_\gamma = 0.4980$. If $v_{xyz}|_E$ equals $u_D|_E$ at $\mathcal{N}(E)$ and $\operatorname{mid}(E)$ for all $E \in \mathcal{E}(\partial\Omega)$, w_D can be designed on the red-refined triangulation with halved edge lengths and accordingly reduced constant $C_\gamma = 0.4980/2^{3/2} = 0.1761$.

E. Projection

This subsection designs a projection operator that projects a given function $v \in P_2(\mathcal{T}; \mathbb{R}^2) \cap \mathcal{A}(\mathcal{T})$ onto a function $\tilde{v} \in P_2(\mathcal{T}; \mathbb{R}^2) \cap \tilde{\mathcal{A}}(\mathcal{T})$. Consider the constrained minimization problem

$$\min_{w \in P_2(\mathcal{T}; \mathbb{R}^2) \cap \tilde{\mathcal{A}}(\mathcal{T})} \sum_{j=1}^J \left((1 + \mu_j) \|\mathbf{D}(v - w)\|_{L^2(\Omega_j)}^2 + (1 + 1/\mu_j) \|\operatorname{div}(v - w)\|_{L^2(\Omega_j)}/c_j^2 \right),$$

where $0 < \mu_j < \infty$ is chosen as follows

$$\mu_j := \begin{cases} \|\operatorname{div} v\|_{L^2(\Omega_j)}/(c_j \|\mathbf{D}_{\text{NC}}(v - u_2)\|_{L^2(\Omega_j)}) & \text{if } v \in \{v_{\text{MP}2(K)}, v_{\text{MP}2\text{CG}3(K)}\}, \\ 1 & \text{otherwise.} \end{cases}$$

For a given enumeration $\mathcal{N} \cup \operatorname{mid}(\mathcal{E}) = \{z_1, \dots, z_M\}$ of the $M := |\mathcal{N}| + |\mathcal{E}|$ nodes of the triangulation, define the index set of all nodes on the boundary

$$\mathcal{M} := \{m \in \{1, \dots, M\} : z_m \in \partial\Omega\}.$$

Let $(\varphi_z : z \in \mathcal{N} \cup \operatorname{mid}(\mathcal{E}))$ denote the piecewise quadratic and globally continuous basis functions of $P_2(\mathcal{T}) \cap C(\bar{\Omega})$ enumerated according to the nodes of the triangulation, i.e. $\varphi_m := \varphi_{z_m}$ for $m = 1, \dots, M$. Let $x, y \in \mathbb{R}^{2M}$ denote the coefficients of the basis representation of w respectively v ,

$$w = \sum_{m=1}^M x_m(\varphi_m, 0)^\top + x_{M+m}(0, \varphi_m)^\top \quad \text{and} \quad v = \sum_{m=1}^M y_m(\varphi_m, 0)^\top + y_{M+m}(0, \varphi_m)^\top.$$

Then, the minimization problem reads

$$\min_{x \in \mathbb{R}^{2M}} (y - x)^\top A (y - x) \quad \text{s.t. } (x_m, x_{M+m})^\top = u_D(z_m) \text{ for } m \in \mathcal{M} \text{ and } Bx = 0,$$

where $A \in \mathbb{R}^{2M \times 2M}$ is defined via

$$A_{\ell m} := \sum_{j=1}^J \left((1 + \mu_j) \int_{\Omega_j} D\varphi_\ell : D\varphi_m \, dx + (1 + 1/\mu_j) \int_{\Omega_j} \operatorname{div} \varphi_\ell \operatorname{div} \varphi_m \, dx / c_j^2 \right)$$

for $\ell, m = 1, \dots, 2M$ and condition (4.1) is expressed by the rectangular matrix $B \in \mathbb{R}^{J \times 2M}$ with the entries

$$B_{jm} = \int_{\partial\Omega_j} \varphi_m \cdot \nu \, ds \quad \text{for } j = 1, \dots, J \text{ and } m = 1, \dots, 2M.$$

Introduce J Lagrangian multipliers $\lambda_1, \dots, \lambda_J$ to ensure the side condition (4.1). Minimizing the Lagrange functional

$$\mathcal{L}(y; x, \lambda) := (y - x)^\top A (y - x) + \lambda^\top B x$$

leads to the saddle point problem

$$\begin{bmatrix} 2A & B^\top \\ B & 0 \end{bmatrix} \begin{bmatrix} x \\ \lambda \end{bmatrix} = \begin{bmatrix} 2Ay \\ 0 \end{bmatrix}.$$

In order to reduce the computational costs, replace the matrix A by its diagonal $\Lambda := \operatorname{diag}(A)$. Finally, define the desired projection

$$\tilde{v} := \sum_{m=1}^M x_m(\varphi_m, 0)^\top + x_{M+m}(0, \varphi_m)^\top \in P_2(\mathcal{T}; \mathbb{R}^2) \cap \tilde{\mathcal{A}}(\mathcal{T}).$$

Remark 4.1. Reference [9] already includes the suggestion of local designs in less detail and proposes to refine such a local bound by solving global problems in the subdomains. This article suggests the usage of the boundary values of the explicit design to decompose the problem.

The novel projection technique is a convenient and more universal alternative that projects any test function $v \in \mathcal{A}(\mathcal{T})$ onto some $\tilde{v} \in \tilde{\mathcal{A}}(\mathcal{T})$ at low costs, e.g. $v \in \mathcal{A}(\mathcal{T})$ might stem from an inexactly solved unconstrained minimization problem as in 4.2 (and so avoids the solve of more expensive saddle point problems) or any nodal interpolation of \hat{u}_{CR} . Another scenario is an inexactly solved Crouzeix-Raviart finite element method where \hat{u}_{CR} is not piecewise divergence-free anymore. In this case the explicit designs presented herein do not satisfy $v \in \tilde{\mathcal{A}}(\mathcal{T})$. Moreover, this projection technique can be generalized to the 3D case, where it is fundamentally more involved to ensure condition (4.1) by simply defining values of the test function as presented in the Subsections IV.A and IV.C.

V. NUMERICAL EXPERIMENTS

This section presents some benchmark examples with convergence history plots for the energy error and history plots of efficiency indices for error estimators as a function of numbers of degrees of freedom (ndof). The labels of the graphs refer to the subscripts of the estimator term η_{xyz} as follows, 'AP2' indicates the piecewise quadratic interpolation v_{AP2} and 'MP2' the minimal piecewise quadratic interpolation v_{MP2} , where the following number in brackets indicates the number

of iterations K in Algorithm 4.1. 'MAred' and 'PMred' indicate the two different piecewise linear interpolations v_{MAred} and v_{PMred} on the red-refined triangulation. The annotation '(mod)' indicates the modified interpolations according to the side condition (4.1) and '(proj)' indicates the usage of the projection from Subsection IV.E. Both allow for the upper bound from Theorem 3.1 (b).

A. Adaptive Algorithm

The benchmark examples employ the following adaptive algorithm which includes an equivalent modification of the a posteriori error estimator η_{opt} from [3] and thus, the generated sequence of discrete solutions and meshes is not biased by one of the investigated estimators. Recall from [4], that this algorithm leads to quasi-optimal convergence in the notion of approximation classes. Undocumented experiments reveal optimal convergence rates of the adaptive algorithms using the error estimators from Section IV as well.

Algorithm 5.1 (APSFEM).

Input Initial regular triangulation \mathcal{T}_0 with refinement edges of the polygonal domain Ω into triangles and bulk parameter $0 < \theta \leq 1$.

for any level $\ell = 0, 1, 2, \dots$ *do*

Solve (3.1)–(3.2) with respect to regular triangulation \mathcal{T}_ℓ with solution (σ_ℓ, u_ℓ) .

Compute $\eta_\ell^2 := \sum_{T \in \mathcal{T}_\ell} \eta_\ell^2(T)$ with

$$\eta_\ell^2(T) := \text{osc}^2(f, T) + |T| \|\text{curl}(\text{dev}\sigma_\ell)\|_{L^2(T)}^2 + |T|^{1/2} \sum_{E \in \mathcal{E}(T)} \|[\text{dev}(\sigma_\ell)\tau_E]_E\|_{L^2(E)}^2$$

Mark a subset \mathcal{M}_ℓ of \mathcal{T}_ℓ of (almost) minimal cardinality $|\mathcal{M}_\ell|$ with

$$\theta \eta_\ell^2 \leq \eta_\ell^2(\mathcal{M}_\ell) := \sum_{T \in \mathcal{M}_\ell} \eta_\ell^2(T).$$

Refine. Compute the smallest regular refinement $\mathcal{T}_{\ell+1}$ of \mathcal{T}_ℓ

with $\mathcal{M} \subseteq \mathcal{T}_\ell \setminus \mathcal{T}_{\ell+1}$ by newest vertex bisection. *od*

Output Sequence of discrete solutions $(\sigma_\ell, u_\ell)_{\ell \in \mathbb{N}_0}$ and meshes $(\mathcal{T}_\ell)_{\ell \in \mathbb{N}_0}$.

B. Classical Example on L-Shaped Domain

The first benchmark problem employs $f(x, y) \equiv 0$ with the exact solution in polar coordinates

$$\begin{aligned} u(r, \vartheta) &= r^\alpha ((1 + \alpha) \sin(\vartheta)w(\vartheta) + \cos(\vartheta)w'(\vartheta), -(1 + \alpha) \cos(\vartheta)w(\vartheta) + \sin(\vartheta)w'(\vartheta))^\top, \\ p(r, \vartheta) &= -r^{\alpha-1} ((1 + \alpha)^2 w'(\vartheta) + w'''(\vartheta)) / (1 - \alpha) \end{aligned}$$

on the L-shaped domain $\Omega = (-1, 1)^2 \setminus ([0, 1] \times [-1, 0])$, where

$$\begin{aligned} w(\vartheta) &= 1/(\alpha + 1) \sin((\alpha + 1)\vartheta) \cos(\alpha\omega) - \cos((\alpha + 1)\vartheta) \\ &+ 1/(\alpha - 1) \sin((\alpha - 1)\vartheta) \cos(\alpha\omega) + \cos((\alpha - 1)\vartheta) \end{aligned}$$

for $\alpha = 856399/1572864$ and $\omega = 3\pi/2$ from [22]. The inhomogeneous Dirichlet boundary data are prescribed by the exact solution $u_D(x, y) := u(x, y)$ on $\partial\Omega$. The L-shaped domain Ω is partitioned into the three unit squares $\Omega_1 = (-1, 0)^2$, $\Omega_2 = (-1, 0) \times (0, 1)$ and $\Omega_3 = (0, 1)^2$. Due to theoretical lower bounds by [10, 11], use $0.1601 \leq c_0$ and $0.3826 \leq c_j$ for $j = 1, 2, 3$.

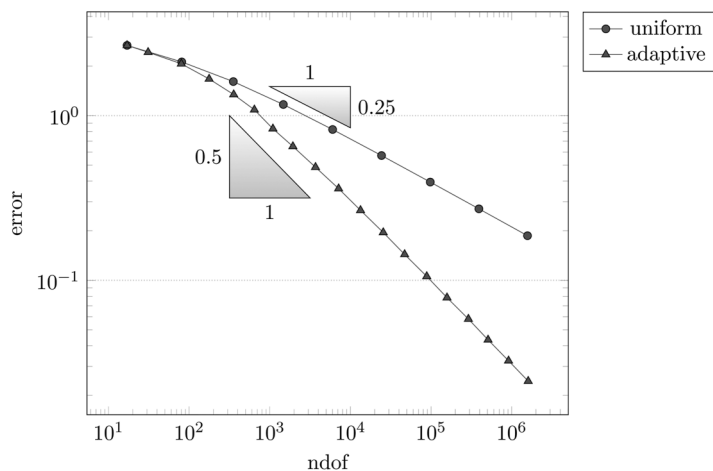


FIG. 2. Convergence history of the energy error for uniform and adaptive mesh refinement for the problem from Subsection V.B.

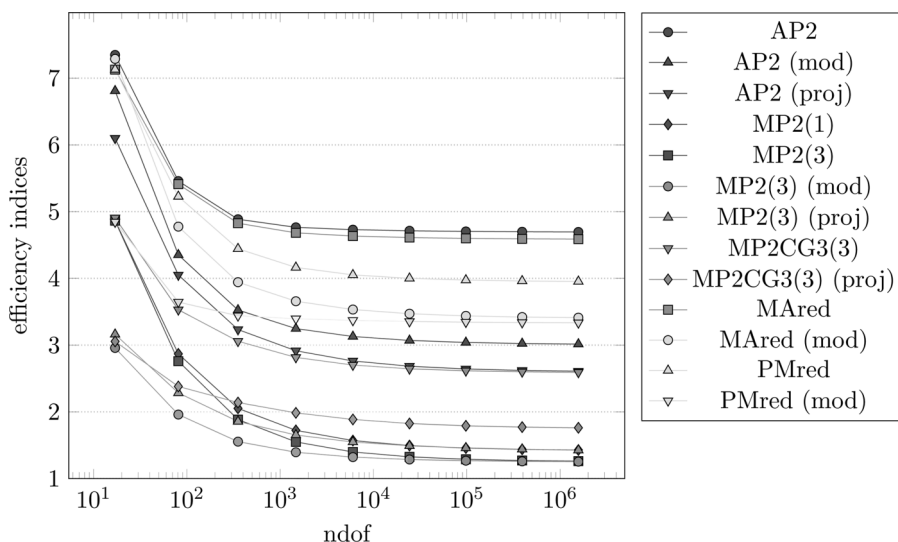


FIG. 3. History of efficiency indices $\eta_{xyz}/\|u - u_h\|$ of various a posteriori error estimators labeled *xyz* in the figure as functions of the number of unknowns on uniform meshes for the problem from Subsection V.B.

Figure 2 shows the convergence history of the exact energy error for uniform and adaptive mesh refinement by Algorithm 5.1 with $\theta = 0.5$. As known for this example, the convergence rate for the uniform mesh refinement is not optimal, i.e. 0.25 with respect to the number of degrees of freedom (or 0.5 with respect to the mesh width as $h \equiv \text{ndof}^{-1/2}$).

Figure 3 shows the efficiency indices for all error estimators for uniform mesh refinement. The main observation is that the efficiency indices for the '(mod)' and '(proj)' error estimators, that allow for the refined upper bounds with the local inf-sup constant from Theorem 3.1 (b), are considerably improved compared to the error estimators that operate with unmodified designs. In

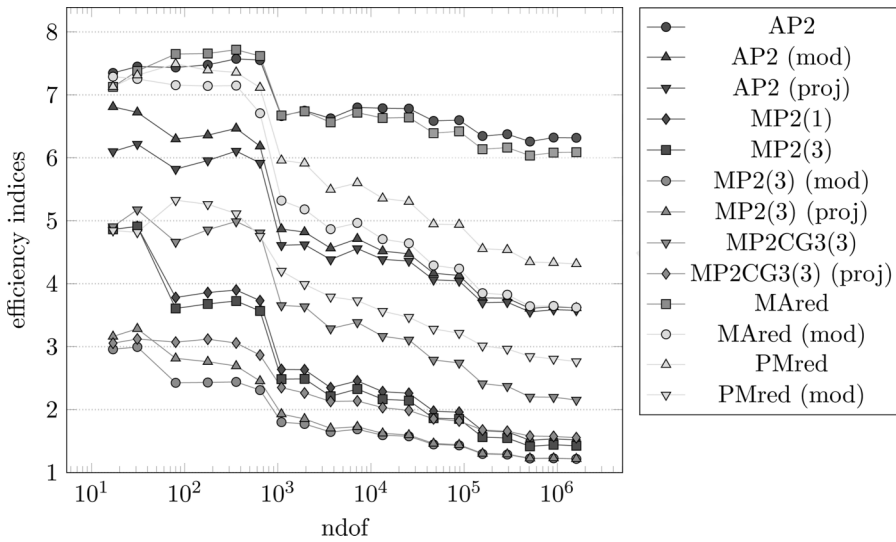


FIG. 4. History of efficiency indices $\eta_{xyz} / \|u - u_h\|$ of various a posteriori error estimators labeled xyz in the figure as functions of the number of unknowns for adaptive mesh refinement for the problem from Subsection V.B.

other words, the gain from the change from global to local inf-sup constants is larger than the loss of freedom from the additional constraints in the designs. As an example the efficiency index for η_{AP2} drops from about 4.5 to almost 3.0 for $\eta_{AP2(mod)}$ and the efficiency index for η_{MAred} drops from 4.4 to about 3.5 for $\eta_{MAred(mod)}$. Also the global designs with a truncated minimization benefit from the modifications and the projection. For example, the efficiency index of $\eta_{MP2CG3(3)}$ of about 2.7 is improved to 1.8 by its modified form $\eta_{MP2CG3(3)(proj)}$. The estimator with the least improvement is $\eta_{MP2(3)}$ which is due to the fact that its inf-sup constant dependable part of the error estimator is very small at least on fine meshes. The variant $\eta_{MP2(3)(proj)}$ is slightly less efficient than the variant $\eta_{MP2(3)(mod)}$. Hence, it seems advisable to add the additional constraint as a side constraint in the minimization problem. However, in case of η_{AP2} , the '(proj)' variant is slightly more efficient than the '(mod)' variant. The efficiency indices for adaptive mesh refinement depicted in Fig. 4 allow similar conclusions with even more remarkable improvements for the local designs.

C. Colliding flow example on stretched domain

Given a ratio $\ell \in \mathbb{N}$, let $\Omega := (-1, 2\ell - 1) \times (-1, 1)$ denote a stretched domain. The subdivision $\Omega_1, \dots, \Omega_\ell$ of Ω consists of the ℓ squares with edge length 2 as displayed in Fig. 5 and lower bounds of the local inf-sup constants $0.3826 \leq c_j$ for $j = 1, \dots, \ell$ from [10, 11]. A computation of a lower bound for the inf-sup constant on star-shaped domains Ω according to [11, Corollary 7 and Proposition 9 i)] yields the lower bounds of c_0 as displayed in Table I.

The second benchmark problem employs $f(x, y) := (240(\ell^{-1}(x + 1) - 1)y^2, 240\ell^{-3}(\ell^{-1}(x + 1) - 1)^2y)^\top$ with the exact solution which is derived by transformation of the solution from the colliding flow example to the stretched domain Ω , i.e.,

$$u(x, y) := (20(\ell^{-1}(x + 1) - 1)y^4 - 4(\ell^{-1}(x + 1) - 1)^5, 20\ell^{-1}(\ell^{-1}(x + 1) - 1)^4y - 4\ell^{-1}y^5)^\top,$$

$$p(x, y) := -20\ell^{-1}(\ell^{-1}(x + 1) - 1)^4 - 2\ell^{-1}y^4.$$

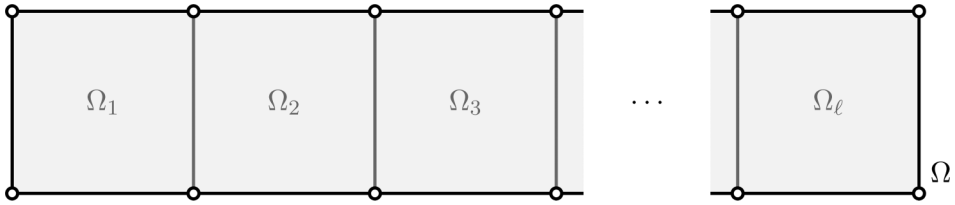


FIG. 5. Subdivision of the domain Ω in the stretched colliding flow example from Subsection V.C.

TABLE I. Efficiency indices for a collection of estimators for the problem from Subsection V.C with different domains for $\ell = 1, 2, 4, 8, 16$. The tables show the results of a computation on the 6 times uniformly red-refined initial triangulation.

ℓ	ndof	AP2	AP2(mod)	MAred	MAred(mod)	PMred	PMred (mod)
1	32,513	2.1455	2.1781	2.7207	2.7610	2.2257	2.2324
2	65,153	3.0522	2.3069	4.3233	3.1558	2.6221	2.1078
4	130,433	4.8789	2.3780	7.5121	3.3666	2.9824	1.9815
8	260,993	8.5031	2.3906	13.6768	3.4124	3.7073	1.9542
16	522,113	15.7631	2.3901	25.9517	3.4199	5.3061	1.9556

ℓ	MP2(3)	MP2(3)(mod)	MP2CG3(3)	MP2CG3(3)(proj)	c_0
1	1.0377	1.0377	1.2131	1.2131	$3.8268 \cdot 10^{-1}$
2	1.0439	1.0280	1.3304	1.2382	$2.2975 \cdot 10^{-1}$
4	1.0520	1.0174	1.5122	1.2489	$1.2218 \cdot 10^{-1}$
8	1.0612	1.0100	1.8327	1.2481	$6.2137 \cdot 10^{-2}$
16	1.0747	1.0057	2.4606	1.2458	$3.1204 \cdot 10^{-2}$

Figure 6 shows the exact error graphs of the 6 computations with varying parameter $\ell = 1, 2, 4, 8, 16$. The error gets worse for larger domains, but its convergence rates stays optimal.

Table I displays the efficiency indices for the computations on a six times red-refined initial triangulation of Ω with $\ell = 1, 2, 4, 8, 16$. In all cases, the error estimators $\eta_{MP2}, \eta_{MP2(mod)}, \eta_{MP2(proj)}$, and $\eta_{MP2CG3(proj)}$ yield the best results with indices between 1 and 2. When the anisotropy of the domain grows, the global versions of the simple estimators $\eta_{AP2}, \eta_{MAred}, \eta_{PMred}$ get worse. For $\ell = 16$, they reveal extremely poor efficiency indices between 15 and 26 (except for η_{PMred}). However, their local versions exhibit almost no change for increasing ℓ . Their efficiency indices range from 1.8 to 3.7. This is due to the deterioration of the inf-sup-constant c_0 for anisotropic domains, which behaves asymptotically like $\mathcal{O}(\ell^{-1})$ [12, Theorem 3].

Table II demonstrates the influence of the modification due to [9] and the projection from Subsection IV.E on the energy error term $\|u_2 - v_{xyz}\|_{NC}$. Both techniques generate almost no increase of the energy error, but can reduce the factor which is related to the inf-sup-constant c_0 significantly, e.g. for anisotropic domains as seen in Table I. This is another evidence for the improvement opportunities of the localization techniques.

D. Backward facing step example

The third benchmark problem employs $f(x, y) \equiv 0$ on the domain $\Omega = ((-2, 8) \times (-1, 1)) \setminus ([-2, 0] \times [-1, 0])$ with Dirichlet boundary data

$$u_D(x, y) = \begin{cases} (-y(y - 1)/10, 0) & \text{if } x = -2, \\ (-y + 1)(y - 1)/80, 0) & \text{if } x = 8, \\ 0 & \text{otherwise} \end{cases}$$

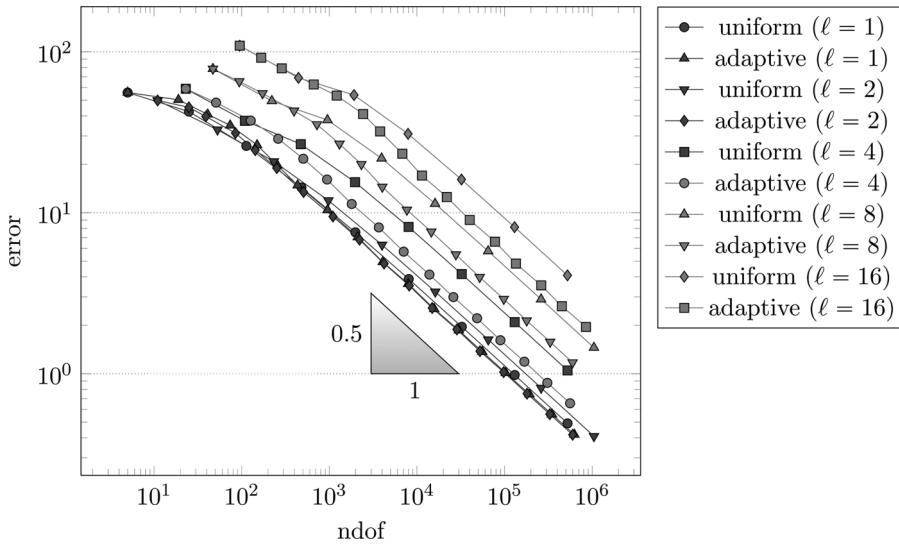


FIG. 6. Convergence history of the exact energy error for uniform and adaptive mesh refinements for the problem from Subsection V.C.

TABLE II. Energy error $\|u_2 - v_{xyz}\|_{NC}$ for a collection of estimators in comparison to the exact error $\|u_2 - u\|_{NC}$ for the problem from Subsection V.C with different domains for $\ell = 1, 2, 4, 8, 16$. The tables show the results of a computation on the six times uniformly red-refined initial triangulation.

ℓ	1	2	4	8	16
ndof	32,513	65,153	130,433	260,993	522,113
AP2	1.98499	1.82007	2.46296	3.46022	4.88960
AP2(mod)	1.98499	1.82016	2.46237	3.45863	4.88676
AP2(proj)	1.98499	1.82007	2.46248	3.45903	4.88751
Exact error	1.95700	1.62876	2.09288	2.90087	4.08394

with a unique, but unknown, weak solution. Therefore the discrete solution on the twice red-refined triangulation is used as a reference solution in the computation of the displayed approximations to the unknown errors. For the refined estimates, the domain Ω is split into six squares as depicted in Fig. 7 with lower bounds of the local inf-sup constants $0.3826 \leq c_j$ for $j = 1, \dots, 6$ from [10, 11]. The lower bound of the inf-sup constant $0.049814 \leq c_0$ in this computation is derived from the formula in [11, Corollary 7]. Up to the authors' knowledge, the assumption in this corollary is not satisfied for Ω . In fact, the true inf-sup constant c_0 might be smaller.

As seen in the previous examples, the adaptive mesh-refinement results in an optimal convergence rate of 0.5 (cf. Fig. 8).

Figures 9 and 10 present the efficiency indices for the error estimators from Section IV. The versions with global inf-sup constant exhibit extremely bad efficiency indices in the range of 8 to 22 for η_{AP2} and η_{MAred} . Significantly better, but still worse are the efficiency indices for η_{PMred} of about 8 to 10 for adaptive mesh refinement. These error estimators are most affected by the very small global inf-sup constant of the specific domain Ω . However, the global version of η_{MP2} still yields good efficiency indices close to 1 because the computed test function v_{MP2} is almost divergence free. Its computationally much cheaper modification η_{MP2CG3} is slightly worse with an index of about 3 for adaptive mesh refinement.

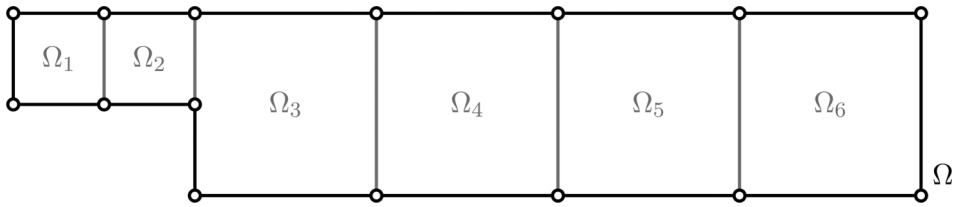


FIG. 7. Subdivision of the domain Ω in the backward facing step example from Subsection V.D.

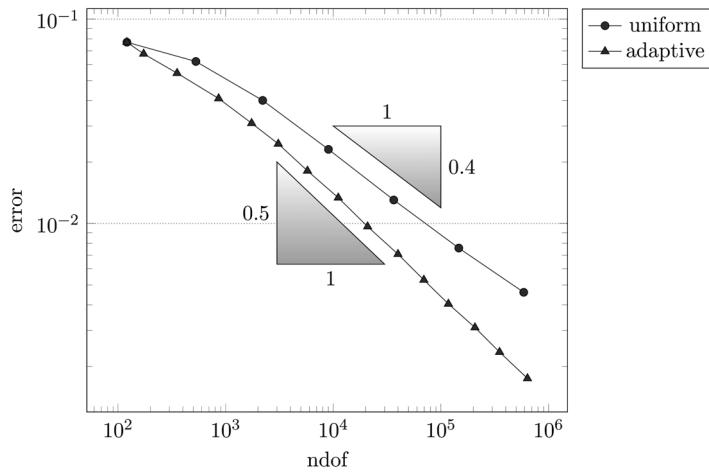


FIG. 8. Convergence history of the energy error with respect to a reference solution on a twice red-refined triangulation for uniform and adaptive mesh refinements for the problem from Subsection V.D.

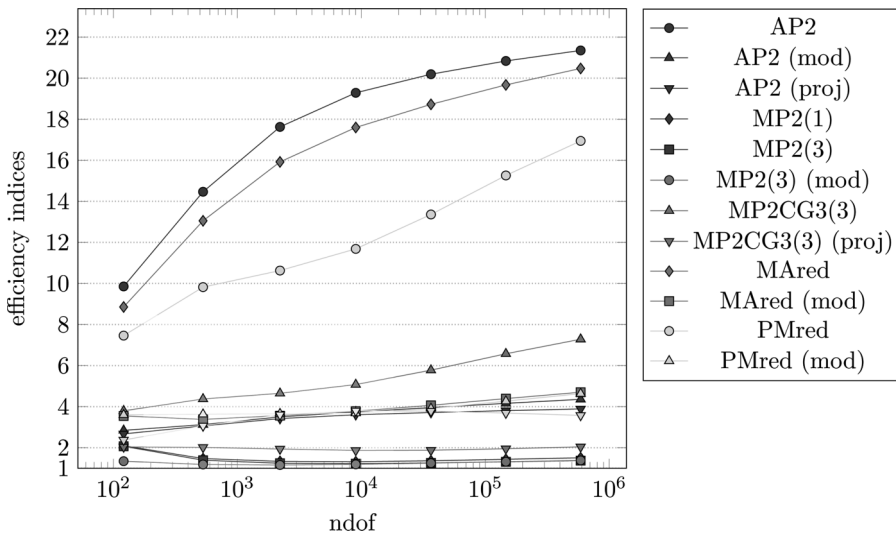


FIG. 9. History of efficiency indices $\eta_{xyz} / \|u - u_h\|$ of various a posteriori error estimators labeled xyz in the figure as functions of the number of unknowns on uniform meshes for the problem from Subsection V.D.

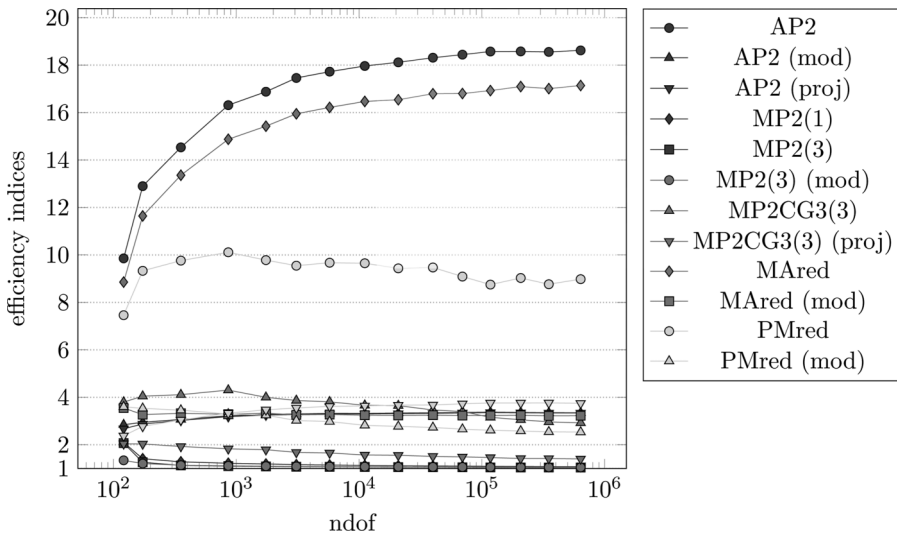


FIG. 10. History of efficiency indices $\eta_{xyz}/\|u - u_h\|$ of various a posteriori error estimators labeled xyz in the figure as functions of the number of unknowns for adaptive mesh refinement for the problem from Subsection V.D.

This benchmark problem once again highlights the exceptional superiority of the proposed designs based on the division of Ω into subdomains and the computation with local inf-sup constants by Theorem 3.1 (b) as suggested by [9]. From the very beginning the estimators with local modification or projection exhibit efficiency indices below 5 in the uniform case and below 4 in the adaptive case. Even the index of the moderate estimator η_{MP2CG3} can be drastically reduced by a factor of at least 2 by using the projected version. It is also remarkable that the computationally cheap but localized upper bounds $\eta_{AP2(mod)}$, $\eta_{AP2(proj)}$, $\eta_{MAred(mod)}$, and $\eta_{PMred(mod)}$ compare favorably well with the global estimator η_{MP2CG3} .

References

1. Z. Cai, B. Lee, and P. Wang, Least-squares methods for incompressible Newtonian fluid flow: linear stationary problems, *SIAM J Numer Anal* 42 (2004), 843–859 (electronic). MR 2084238 (2005i:65180)
2. Z. Cai and Y. Wang, A multigrid method for the pseudostress formulation of Stokes problems, *SIAM J Sci Comput* 29 (2007), 2078–2095 (electronic). MR 2350022 (2008g:65156)
3. C. Carstensen, D. Kim, and E-J. Park, A priori and a posteriori pseudostress-velocity mixed finite element error analysis for the Stokes problem, *SIAM J Numer Anal* 49 (2011), 2501–2523. MR 2873244
4. C. Carstensen, D. Gallistl, and M. Schedensack, Quasi-optimal adaptive pseudostress approximation of the stokes equations, *SIAM J Numer Anal* 51 (2013), 1715–1734. MR 3066804
5. C. Carstensen and C. Merdon, Estimator competition for Poisson problems, *J Comput Math* 28 (2010), 309–330.
6. C. Carstensen and C. Merdon, Effective postprocessing for equilibration a posteriori error estimators, *Numer Math* 123 (2013), 425–459. MR 3018142
7. C. Carstensen and C. Merdon, Computational survey on a posteriori error estimators for nonconforming finite element methods for the Poisson problem, *J Comput Appl Math* 249 (2013), 74–94. MR 3037808

8. M. Ainsworth and W. Dörfler, Reliable a posteriori error control for nonconformal finite element approximation of Stokes flow, *Math Comp* 74 (2005), 1599–1619 (electronic).
9. K-Y. Kim, Fully computable a posteriori error estimates for the Stokes equation without the global inf-sup constant, *Comput Math Appl* 67 (2014), 681–691. MR 3149741
10. G. Stoyan, Towards discrete Velté decompositions and narrow bounds for inf-sup constants, *Comput Math Appl* 38 (1999), 243–261.
11. M. Dauge, C. Bernardi, M. Costabel, and V. Girault, On Friedrichs constant and Horgan-Payne angle for LBB condition, *Twelfth International Conference Zaragoza-Pau on Mathematics, Monogr. Mat. García Galdeano*, vol. 39, Prentice Univ. Zaragoza, Zaragoza, 2014, pp. 87–100. MR 3205184
12. M. A. Ol’shanskiĭ and E. V. Chizhonkov, On the best constant in the inf-sup condition for elongated rectangular domains, *Mat Zametki* 67 (2000), 387–396. MR 1779472 (2001g:76020)
13. C. Carstensen and C. Merdon, Computational survey on a posteriori error estimators for the Crouzeix–Raviart nonconforming finite element method for the Stokes problem, *Comput Methods Appl Math* 14 (2014), 35–54. MR 3149616
14. A. Hannukainen, R. Stenberg, and M. Vohralík, A unified framework for a posteriori error estimation for the Stokes problem, *Numer Math* 122 (2012), 725–769. MR 2995179
15. A. Agouzal, A posteriori error estimator for nonconforming finite element methods, *Appl Math Lett* 7 (1994), 61–66.
16. E. Dari, R. G. Duran, C. Padra, and V. Vampa, A posteriori error estimators for nonconforming finite element methods, *RAIRO Modél Math Anal Numér* 30 (1996), 385–400.
17. S. Bartels, C. Carstensen, and S. Jansche, A posteriori error estimates for nonconforming finite element methods, *Numer Math* 92 (2002), 233–256.
18. C. Carstensen, D. Gallistl, and M. Schedensack, L^2 best-approximation of the elastic stress in the Arnold–Winther FEM, Preprint 2014–15, Humboldt-Universität zu Berlin, Institut für Mathematik, 2014.
19. D. Braess, *Finite elements - theory, fast solvers, and applications in solid mechanics*, Cambridge University Press, New York, 2007.
20. R. S. Laugesen and B. A. Siudeja, Minimizing Neumann fundamental tones of triangles: An optimal Poincaré inequality, *J Differential Equations* 249 (2010), 118–135. MR 2644129 (2011f:35238)
21. S. Bartels, C. Carstensen, and G. Dolzmann, Inhomogeneous Dirichlet conditions in a priori and a posteriori finite element error analysis, *Numer Math* 99 (2004), 1–24.
22. R. Verfürth, A posteriori error estimators for the Stokes equations, *Numer Math* 55 (1989), 309–325.